Pergamon

Acta mater. 49 (2001) 13–20

Acta MATERIALIA

www.elsevier.com/locate/actamat

INFLUENCE OF AN APPLIED STRAIN FIELD ON MICROSTRUCTURAL EVOLUTION DURING THE $\alpha_2 \rightarrow O$-PHASE TRANSFORMATION IN Ti–Al–Nb SYSTEM

Y. H. WEN[1, 2]*, Y. WANG[2] and L. Q. CHEN[1]

[1]Department of Materials Science and Engineering, The Pennsylvania State University, University Park, PA 16802, USA and [2]Department of Materials Science and Engineering, The Ohio State University, 2041 College Road, Columbus, OH 43210, USA

(Received 15 May 2000; received in revised form 14 August 2000; accepted 5 September 2000)

Abstract—We investigate the influence of an applied homogeneous strain on the coherent α_2 (DO_{19}) to *O*-phase transformation in Ti–Al–Nb alloys using a phase-field approach. The emphasis is on the effect of the applied strain on the two-phase morphology, as well as the equilibrium volume fractions of different orientation domains of the *O*-phase. It is found that the applied homogeneous strain field does not change the essential features of the morphological patterns, but does alter the relative amount of each orientation domain and the equilibrium volume fraction of the *O*-phase. When the applied strain is of the same order of magnitude as the stress-free transformation strain, the initial two-phase mixture becomes unstable and transforms into a single *O*-phase.

Keywords: Ti–Al–Nb alloys; Microstructure; Applied strain field; Computer simulation; Phase transformations

1. INTRODUCTION

A hexagonal to orthorhombic transformation is accompanied by a crystal lattice symmetry change which produces three types of orientation variants of the orthorhombic phase (*O*-phase) if the orientation relationships between the two phases are: $(001)_o//(0001)_h$; $[100]_o//[2\bar{1}10]_h$. If the transformation is coherent, the elastic interactions arising from the lattice mismatch between the product and matrix phases may change the orientation relationship to provide an invariant plane condition which minimizes the elastic energy. This will alter the number of orientation variants as occurs, for example, in the α_2 (DO_{19}) to *O*-phase transformation in Ti–Al–Nb [1] where a clockwise rotation and a counter clockwise rotation of a small angle of the three original variants produce three pairs of nearly orthogonal orientation variants with new orientation relationships, as has been described by Muraleedharan and Banerjee [1].

Accommodation of the long-range elastic interactions between the high-symmetry and low-symmetry phases, as well as among different orientation domains of the low symmetry phase, usually lead to very complex self-accommodating morphological patterns. Extensive experimental studies have been carried out to study the morphological patterns formed during annealing of Ti–Al–Nb alloy in which simultaneous decomposition and ordering lead to a mixture of α_2 and *O*-phases [1–4]. Recently, using the phase-field approach, we systematically investigated the microstructural evolution during a hexagonal to orthorhombic transformation [4–6]. Our simulations were able to predict all the complex morphological patterns observed in the experiments [5, 6] as well as some new features. Examples of the predicted morphological patterns are schematically shown in Figs 1 and 2 for high and low volume fractions of the *O*-phase, respectively. In these figures, different filling patterns are used to distinguish the three different pairs of orientation variants. It is interesting to note that the morphological patterns could be very different depending on the number of variants present. All the interfaces between the α_2 and the *O*-phase are found to be undistorted habit planes of the type $\{470\}_O$, and the domain boundaries between different orientation variants of the *O*-phase are twin boundaries of either $\{110\}_O$ or $\{130\}_O$, which agree well with experimental observations [3, 4].

A coherent multi-phase and multi-domain microstructure is inherently sensitive to an applied stress or

* To whom all correspondence should be addressed. Tel.: +1-614-688-5616; fax: +1-614-292-1537.

E-mail address: wen@bentley.eng.ohio–state.edu (Y. H. Wen)

1359-6454/01/$20.00
PII: S1359-6454(00)00306-2

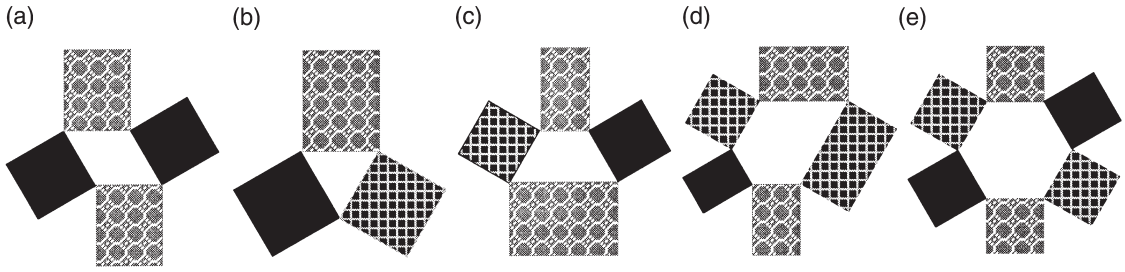

Fig. 1. Schematic presentation of the collective morphological patterns observed in computer simulation of $\alpha^2 \rightarrow O$-phase transformation in a Ti–Al–Nb alloy of relatively high volume fraction of the product phase. Different filling patterns represent three different pairs of orientation variants of the *O*-phase.

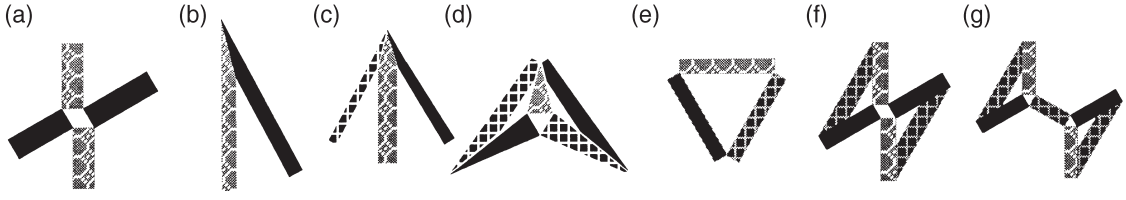

Fig. 2. Schematic simulated patterns with relatively low volume fraction of *O*-phase in an α_2 matrix. Both domain/domain and domain/matrix interfaces are involved.

strain field. In the absence of any external field, the volume fraction of each orientation variant of the *O*-phase in a α_2 + O two-phase mixture statistically should be the same since all the variants are energetically degenerate. Moreover the presence of all the orientation variants is necessary to fully accommodate the misfit strain. When an external stress or strain field is applied, the stress-free transformation strain associated with the α_2 and each orientation variant of the *O*-phase interacts differently with the applied field. As a result, even in the case of a homogeneous modulus, an external strain should modify the relative amount of the α_2 and *O*-phase as well as the relative amount of the different orientation variants of the *O*-phase, and hence change the morphology of the multiphase and multi-variant mixture. In this paper we focus on the influence of an applied strain field on the microstructural development in two Ti–Al–Nb alloys during the α_2 to *O*-phase transformations.

2. PHASE-FIELD APPROACH

In our previous phase-field modeling of the $\alpha_2 \rightarrow O$-phase transformation without external field, three long-range order (*lro*) parameters, $\eta_1(\mathbf{r}, t)$, $\eta_2(\mathbf{r}, t)$, and $\eta_3(\mathbf{r}, t)$ (where $\mathbf{r}$ is the spatial coordinate vector) were introduced to describe the spatial distribution of the three pairs of orientation variants of the *O*-phase. The composition difference between the α_2 and the *O*-phase is described by the concentration field, $c(\mathbf{r}, t)$. The spatio-temporal evolution of these variables describes the microstructural evolution. The temporal evolution of the *lro* parameters can be obtained by solving the time-dependent Ginzburgh–Landau equation.

$$\frac{\partial \eta_p(\mathbf{r}, t)}{\partial t} = -L\frac{\delta F}{\delta \eta_p(\mathbf{r}, t)} + \xi_p(\mathbf{r}, t);\ p = 1, 2, 3, \tag{1}$$

while the temporal evolution of the concentration field can be described by the non-linear Cahn–Hilliard diffusion equation

$$\frac{\partial c(\mathbf{r}, t)}{\partial t} = M\nabla^2\frac{\delta F}{\delta c(\mathbf{r}, t)} + \xi(\mathbf{r}, t), \tag{2}$$

where L and M are kinetic coefficients characterizing structural relaxation and diffusional mobility, F is the total free energy of the system, $\xi_p(\mathbf{r}, t)$ and $\zeta(\mathbf{r}, t)$ are Langivin random noise terms which are related to thermal fluctuations in the *lro* parameter and composition, respectively. They are assumed to be Gaussian distributed and their correlation properties meet the requirements of the fluctuation-dissipation theorem [7].

To present the kinetic equations in an explicit analytical form suitable for numerical solution, the total free energy F needs to be expressed as a functional of the concentration and *lro* parameter fields. For coherent transformations, the total free energy consists of both the chemical free energy (F_{ch}) and the elastic strain energy (E_{el}) contributions. The non-equi-

librium chemical free energy as a functional of the field variables can be approximated using a coarse-grained Landau–Ginzburg free energy functional,

$$F_{\text{ch}} = \int_V \left[\frac{1}{2}\rho(\nabla c)^2 + \frac{1}{2}\lambda \sum_{p=1}^{3} (\nabla \eta_p)^2 + f(c, \eta_1, \eta_2, \eta_3) \right] \mathrm{d}V \tag{3}$$

where ρ and λ are gradient energy coefficients. The integration in equation (3) is carried out over the entire system volume V. The gradient terms in equation (3) provide an energy penalty to inhomogeneities in composition and *lro* parameters which take place mainly at the interfaces. The local specific free energy $f(c_1, \eta_1, \eta_2, \eta_3)$ in equation (3) defines the basic bulk thermodynamic properties of the system. It is approximated by a Landau-type expansion polynomial,

$$F(c, \eta_1, \eta_2, \eta_3) = \frac{A_1}{2}(c-c_1)^2 + \frac{A_2}{2}(c_2 - c) \sum_{p=1}^{3} \eta_p^2 - \frac{A_3}{4} \sum_{p=1}^{3} \eta_p^4 + \frac{A_4}{6} \Big(\sum_{p=1}^{3} \eta_p^2 \Big)^3, \tag{4}$$

where c_1 and c_2 are constants close to the equilibrium concentrations for the parent α_2 phase and product O-phase, respectively; A_1–A_4 are four positive phenomenological constants which are employed to fit the local specific free energy to available experimental data. All these phenomenological constants are assumed to be the same as those employed in a recent work dealing with the same phase transformation without the influence of an applied field [4]. When values of all the *lro* parameters are zero, it describes the compositional dependence of the free energy of the parent phase. At a given composition, the local free energy has three degenerated minima corresponding to the free energy of the three pairs of orientation variants. The free energy as a function of composition for both the parent α_2 phase and the precipitate O-phase is shown in Fig. 3, which is similar to that proposed by Bendersky *et al*. [8].

The elastic strain energy of a coherent multi-phase and multi-domain mixture can be expressed as [9, 10]

$$\begin{aligned} E_{\text{el}} = {} & \frac{V}{2} C_{ijkl} \bar{\epsilon}_{ij} \bar{\epsilon}_{kl} \\ & - V C_{ijkl} \bar{\epsilon}_{ij} \sum_{p=1}^{3} \epsilon_{kl}^{\text{o}}(p) \overline{\eta_p^2(\mathbf{r})} \\ & + \frac{V}{2} C_{ijkl} \sum_{p=1}^{3} \sum_{q=1}^{3} \epsilon_{ij}^{\text{o}}(p) \epsilon_{kl}^{\text{o}}(q) \overline{\eta_p^2(\mathbf{r}) \eta_q^2(\mathbf{r})} \\ & - \frac{1}{2} \sum_{p=1}^{3} \sum_{q=1}^{3} \int \frac{d^3\mathbf{g}}{(2\pi)^3} B_{pq}(\mathbf{n}) \{\eta_p^2(\mathbf{r})\}_{\mathbf{g}}^{*} \{\eta_q^2(\mathbf{r})\}_{\mathbf{g}} \end{aligned} \tag{5}$$

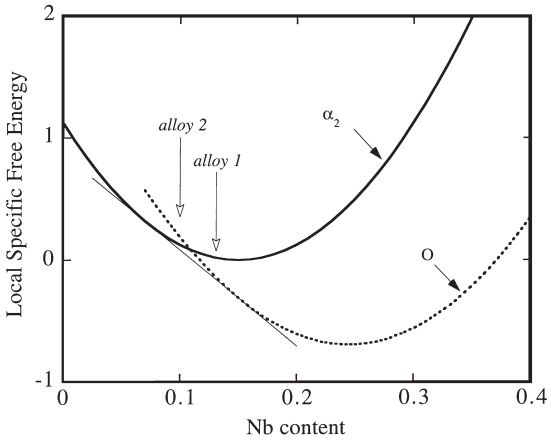

Fig. 3. Local specific free energy for parent and product phases as a function of the content of Nb.

In equation (5), $\overline{(\ldots)}$ represents the volume average of $(\ldots)$, V is the total volume of the system, C is the elastic moduli tensor, $\bar{\epsilon}_{ij}$ is the macroscopic homogeneous strain, $\epsilon^{\text{o}}(p)$ is the stress-free transformation strain tensor of orientation variant p of the O-phase when the corresponding order parameter assumes its equilibrium value, i.e. $\eta_p^2(\mathbf{r}) = 1$. $B_{pq}(n)$ is a two-body elastic interaction potential given by

$$B_{pq}(\mathbf{n}) = n_i \sigma_{ij}^{\text{o}}(p) \Omega_{jk}(\mathbf{n}) \sigma_{kl}^{\text{o}}(q) n_l \tag{6}$$

where $\mathbf{n} = \mathbf{g}/g$ is a unit vector in reciprocal space and n_i is its ith component, $\sigma_{ij}^{\text{o}}(p) = C_{ijkl}\epsilon_{kl}^{\text{o}}(p)$, and $\Omega_{ij}(n)$ is a Green function tensor which is inverse to the tensor $\Omega_{ij}^{-1}(\mathbf{n}) = C_{iklj} n_k n_l$, $\{\eta_q^2(\mathbf{r})\}_{\mathbf{g}} = \int \frac{d^3\mathbf{g}}{(2\pi)^3} \eta_q^2(\mathbf{r}) \exp(-i\mathbf{g}\cdot\mathbf{r})$ is the Fourier transform of $\eta_q^2(\mathbf{r})$ and $\{\eta_p^2(\mathbf{r})\}_{\mathbf{g}}^{*}$ is the complex conjugate of $\{\eta_p^2(\mathbf{r})\}_{\mathbf{g}}$. The readers are referred to Refs [5, 6] for more details.

The first two terms on the right-hand side of the above equation describe the elastic energy due to a homogeneous deformation. The third term describes the elastic energy associated with deforming the stress-free product phase back into its geometrical shape before the transformation. The last term describes the heterogeneous relaxation of the precipitates and matrix which does not produce any macroscopic shape change but affects the shape, size and spatial distribution of the precipitates. In this work, we limit ourselves to the case when the whole system is subject to a homogeneous applied strain. For this particular case, $\bar{\epsilon}_{ij}$ is equal to the applied strain $\epsilon_{ij}^{\text{applied}}$ [10].

3. SIMULATION RESULTS AND DISCUSSION

As pointed out in our previous work [4–6] the microstructure associated with the

hexagonal→orthorhombic transformation is pseudo-two-dimensional. Parallel rods (or plates in the case of low volume fractions) of orthorhombic phase are directed along the normal of the close-packed plane $(0001)_{hcp}$. In this case, we can simply focus on the microstructure evolution on the $(0001)_{hcp}$ plane. Therefore, all the simulations performed in this work are carried out on 2D systems of 1024×1024 mesh points. Assuming that the microstructure is macroscopically homogeneous, a periodical boundary condition is imposed along both dimensions. The initial condition for the simulation is a homogeneous hexagonal phase described by

$$c(\mathbf{r}) = \bar{c};\ \eta_1(\mathbf{r}) = 0,\ \eta_2(\mathbf{r}) = 0,\ \eta_3(\mathbf{r}) = 0,$$

where $\bar{c}$ is the mean composition of Nb. The kinetic equations are solved numerically in the Fourier space using a semi-explicit algorithm [11].

As indicated by the common tangent in Fig. 3, the equilibrium compositions for the two-phase mixture without considering the influence of the elastic strain energy are 7% and 15% Nb (at.%) for α_2 and O-phase, respectively. In order to study the morphological features with different fractions of the product O-phase under the applied strain field, two alloys with different Nb compositions are selected (see Fig. 3).

When an external strain is applied, the applied strain and the stress-free transformation strains are coupled. This coupling is described by $-C_{ijkl}\bar{\epsilon}_{ij}\sum_{p=1}^{3} \epsilon^{o}_{kl}(p)\overline{\eta_p^2(\mathbf{r})}$ in equation (5). Since the three pairs of orientation variants have different stress-free transformation strains in the global frame coordinate [6], this coupling term has different values for different orientation variants and thus promotes or suppresses the growth of certain orientation variants. As a result, the growth of the domains becomes selective.

For simplicity, we apply a homogeneous uniaxial strain to investigate its influence on the microstructural evolution. The strain is applied along such a direction that the first two pairs of orientation variants are equally favored, while pair 3 is unfavored. In the simulation, the total homogeneous strain is kept constant and is given by

$$\bar{\boldsymbol{\epsilon}} = \epsilon^{\mathrm{amp}} \begin{pmatrix} 3/4 & \sqrt{3}/4 \\ \sqrt{3}/4 & 1/4 \end{pmatrix}, \qquad (7)$$

where ϵ^{amp} is the amplitude of the homogeneous strain which contains the applied elastic strain and the homogeneous strain due to the phase transformation and microstructure changes induced by the applied strain. The total homogeneous strain is given in the unit of the shear magnitude of the stress-free transformation strain, ϵ_s [4–6]. The simulation results are presented in Figs 4, 7 and 9 , where different gray levels are used to distinguish the O-phase and the parent α_2 phase as well as the different pairs of the orientation variants of the O-phase. The gray levels in thesefigures represent the values of $(\eta_1^2 - \eta_2^2 - 2\times\eta_3^2)$; the higher the values, the brighter the shade. Therefore, the four different gray levels from brightest to darkest correspond to pair 1, parent α_2 phase, pair 2 and pair 3, respectively.

3.1. Precipitation under an applied strain

As shown in Fig. 3, alloy 1 has an average composition of 12.5% and the equilibrium volume fraction of the O-phase is 69% without considering the effect of coherency strain. The effect of the applied strain field on the microstructure developed at the reduced time $\tau = 200$, at which the volume fraction of each phase is close to its equilibrium value (i.e. no significant change with time), is shown in Fig. 4. When the applied strain is 1/10 of the typical shear deformation of the O-phase [Fig. 4(a)], the resulting microstructural patterns look quite similar to those obtained from a precipitation process without an external field [4]. However, a close examination of the microstructure reveals that the volume fractions of pairs 1 and 2 are significantly higher than that of pair 3 (Fig. 5), while the total amount of the precipitates is only slightly higher than what was observed in the case without an external field [4]. This result demonstrates a selective growth of orientation variants due to the applied strain field. It should be pointed out that the growth in real alloys may occur through a ledge mechanism and the externally applied strain field may affect ledge nucleation and migration leading to selective growth. This detailed atomistic mechanism is difficult to consider in the framework of the continuum phase field model employed in this study unless detailed knowledge on how the ledge nucleation and migration rates are related to the macroscopic mobilities of the interfaces are known. However, the main simulation results obtained concerning the effect of the applied strain on the morphology and the equilibrium volume fraction of the orthorhombic phase should not be affected.

If we further increase the applied strain to 1/4 of ϵ_s, the total volume fraction of the precipitates increases slightly while the difference in volume fraction between the two pairs of favored orientation variants and the unfavored pair 3 changes dramatically, which is clearly shown in Fig. 5. As a result, the volume fraction of pair 3 is much lower than that observed in the case without an external field and the microstructure patterns are dominated by the simplest zigzag pattern consisting of two pairs of orientation variants, as shown in Fig. 1(a). The combination of the zigzag patterns leads to a typical stair-like morphology. In locations where pair 3 is present, all those patterns shown in Figs 1(b)–(e) can still be found.

When the applied strain is further increased up to a half of the typical shear deformation [Fig. 4(c)], pair

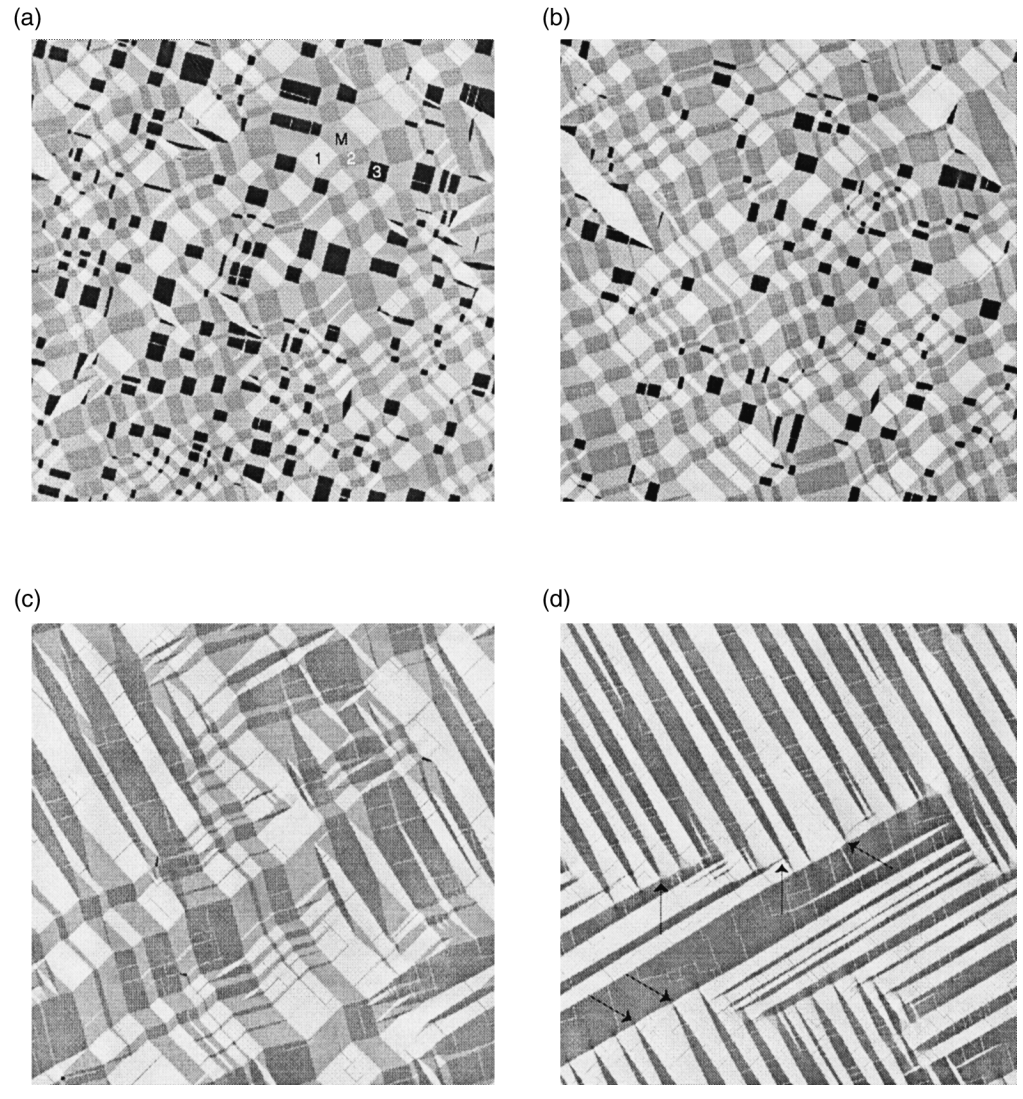

Fig. 4. Simulated microstructure at $\tau = 200$ for precipitation under different levels of applied strain. The mean composition of the Ti–Al–Nb alloy contains 12.5 at.% Nb. In (a), *M* represents α_2, and 1–3, three pairs of orientation variants of the *O*-phase. (a) $\epsilon^{amp} = 0.1\epsilon_s$; (b) $\epsilon^{amp} = 0.25\epsilon_s$; (c) $\epsilon^{amp} = 0.5\epsilon_s$ and (d) $\epsilon^{amp} = 1.0\epsilon_s$

.

3 completely disappears and the resulting microstructure is significantly different from those obtained in the previous simulations. The dominant morphology for a single precipitate changes to a long band from the original square-like block. The corresponding microstructural patterns are rather simple. They can be described by those shown in Figs 2(a) and (b), which have been observed in alloys with low volume fractions of the precipitate phase under no external field [4]. Further increase in the applied strain up to the same amount as the typical shear deformation results in a single product phase consisting of evenly distributed long strips of pairs 1 and 2 [Fig. 4(d)]. The formation of such a single-phase microstructure in a two-phase alloy indicates that the influence of the external field on the phase equilibrium is dominant over that of the chemical free energy. It should be pointed out that an applied strain of the same magnitude as ϵ_s may correspond to a very high strain and the material under consideration may not be within the elastic deformation regime anymore. The above results may, however, serve as an upper limit of how the microstructure responds to an increasing applied strain. It may also be worth noting that the formation of some sharp tips at the intersection area [for example, see those areas indicated by black arrows in Fig. 4(d)] is a result of minimizing the elastic energy, as pointed out in a previous work [6].

It is interesting to note that some of the experimentally observed two-phase microstructures in Ti–Al–Nb alloys without explicitly applying an external strain or stress field are similar to those predicted in our simulations with an external strain field. An example is shown in Fig. 6 [4], in which 1~3 denote

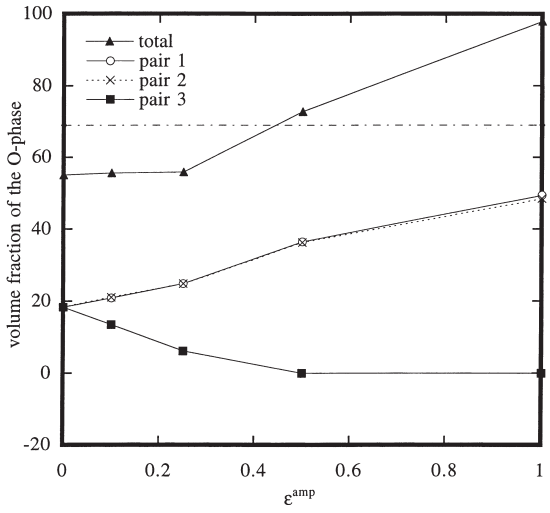

Fig. 5. Influence of the magnitude of an applied strain on the volume fractions of the product *O*-phase and its three pairs of orientation variants corresponding to the final configuration, as shown in Fig. 4. The dot and dashed line represents the anticipated total volume fraction of the *O*-phase in the case without elastic interaction.

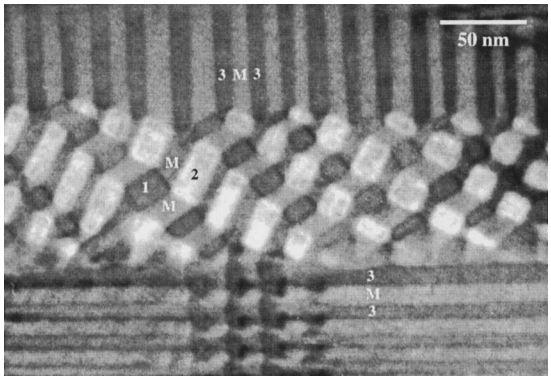

Fig. 6. TEM micrograph of a two-phase microstructure (α_2 + *O*-phase) in the Ti–Al–Nb alloy.

the three pairs of orientation variants of the *O*-phase and *M* denotes the matrix (α_2 phase). It can be seen that distribution of the three pairs of orientation variants is highly inhomogeneous. The central part of the micrograph consists of mainly pairs 1 and 2, while the rest is dominated by pair 3. We have shown that without an external field, the misfit strain is most effectively accommodated when all three pairs of orientation variants are present [4]. Therefore, as originally suggested by Bendersky [12], a non-uniform distribution of the three pairs of orientation variants, as it occurs in Fig. 6, could be from a local inhomogeneous stress distribution.

The above results are obtained for a relatively higher volume fraction of the *O*-phase. In alloy 2, where the average composition is 10 at.% Nb (Fig. 3), the equilibrium volume fraction of the stress free *O*-phase is about 37%. The microstructures obtained under different magnitudes of the applied strain field are shown in Fig. 7. The general effect of the applied strain on the microstructural evolution is similar to that observed in alloy 1. When the applied strain is relatively small, one can find all the basic morphological patterns (motifs) shown in Fig. 2, which were observed in the same system without an applied field [4]. However, when the applied strain is increased to $1/4\epsilon_s$, pair 3 (black) is dropping out while pairs 1 and 2 are becoming dominant. Accordingly, the basic morphological patterns observed in the presence of all three pairs of orientation variants [Figs 2(c)–(f)] disappear. The dominant morphological patterns are those shown in Figs 2(a) and (b), which are based upon the contact of two pairs of orientation variants. When the applied strain further increases to a higher level, e.g. $1/2\epsilon_s$ [Fig. 7(c)] and $1.0\epsilon_s$ [Fig. 7(d)], the microstructures are roughly the same as those predicted for alloy 1 containing 12.5 at.% Nb [Figs 4(c) and (d)]. These results indicate that the transformations are controlled by the accommodation of the applied strain.

3.2. Influence of applied strain on two-phase equilibrium

The study of thermodynamics of stressed crystals was pioneered by Larché and Cahn [13]. In a coherent system, the equilibrium state of a phase is determined by minimization of the total free energy, which contains the elastic strain energy [9, 14]. Since the elastic energy depends sensitively on the mesoscopic morphological patterns, the equilibrium volume fraction of the coherent phases will depend on the degree of elastic strain accommodation of a particular morphological pattern. For example, our previous simulation on a coherent hexagonal to orthorhombic transformation concluded that the transformation cannot go to completion when any one of the three pairs of orientation variants is absent (see Figs 4–6 in [6]). For the $\alpha_2 \rightarrow O$-phase transformation considered here, the total volume fraction of the precipitates without an external field is about 55% (see the value indicated by the black triangle at $\epsilon^{amp} = 0$ in Fig. 5), which is much lower than the equilibrium volume fraction (69%) predicted by the stress-free *f–c* plot (Fig. 3). When an external strain field is applied, the equilibrium volume fraction is further altered because of the coupling between the internal stress field and the applied field. As predicted in our computer simulation shown in the previous section the applied strain has a strong effect on the equilibrium volume fraction of the precipitate phase.

The effect of the applied strain on the two-phase equilibrium can be understood by examining the coupling term,

$$-C_{ijkl}\bar{\epsilon}_{ij}\sum_{p=1}^{3}\epsilon^{0}_{kl}(p)\overline{\eta_p^2(\mathbf{r})}$$

in equation (5). In contrast to the last two terms in

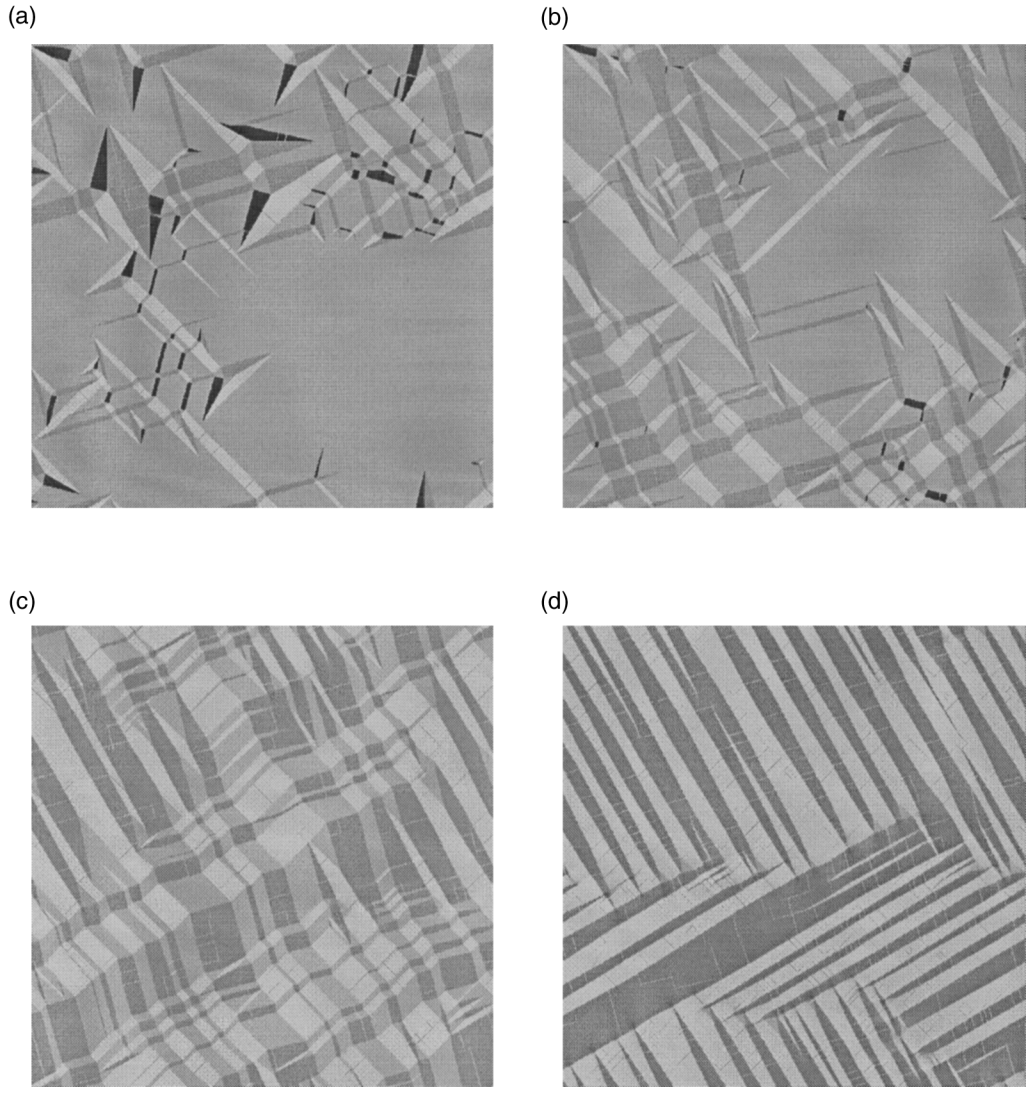

Fig. 7. Simulated microstructure at $\tau = 200$ for precipitation under different levels of applied strain. The mean composition of the Ti–Al–Nb alloy contains 10.0 at.% Nb. (a) $\epsilon^{amp} = 0.1\epsilon_s$; (b) $\epsilon^{amp} = 0.25\epsilon_s$; (c) $\epsilon^{amp} = 0.5\epsilon_s$ and (d) $\epsilon^{amp} = 1.0\epsilon_s$.

equation (5), this coupling term is configuration-independent. Therefore, a qualitative analysis can be made by simply adding this term to the local specific free energy in equation (4). Figure 8 illustrates the effect of addition of this term on the *f–c* curves and the equilibrium volume fractions of the parent phase and the three pairs of orientation variants of the *O*-phase. It is readily seen that the applied strain leads to a decrease in the free energy of pairs 1 and 2 [Fig. 8(a)] and an increase for pair 3 [Fig. 8(b)]. The variation is proportional to the magnitude of the applied strain. As a result, the applied strain causes a rotation of the common tangent (CT) lines (see the solid lines between two ● ($\epsilon^{amp} = 1.0\epsilon_s$) and between two ⊙ ($\epsilon^{amp} = 0$) which leads to an increase in the equilibrium volume fraction of pairs 1 and 2 and a decrease in the equilibrium fraction of pair 3. The total volume fraction of all three pairs of orientation variants of the *O*-phase is also a sensitive function of the applied strain field (Fig. 5). For instance, the equilibrium volume fraction of the product phase is predicted to be ~37% for alloy 2 from the *f–c* curve (Fig. 3) without the influence of the elastic energy. However, the microstructure shown in Fig. 7(c) ($0.5\epsilon_s$) contains ~2/3 product phase (pairs 1 and 2) and the one shown in Fig. 7(d) contains ~100% product phase.

We note that different equilibrium volume fractions of the three pairs of orientation variants of the product phase will be expected if the external strain field is applied along a different direction. This has been confirmed by a computer simulation parallel to that shown in Fig. 7(c), in which the original tensile strain ($0.5\epsilon_s$) has been changed to a compressive strain without changing its magnitude. The microstructure predicted at $\tau = 200$ is shown in Fig. 9. Since the applied compressive strain will promote pair 3 and

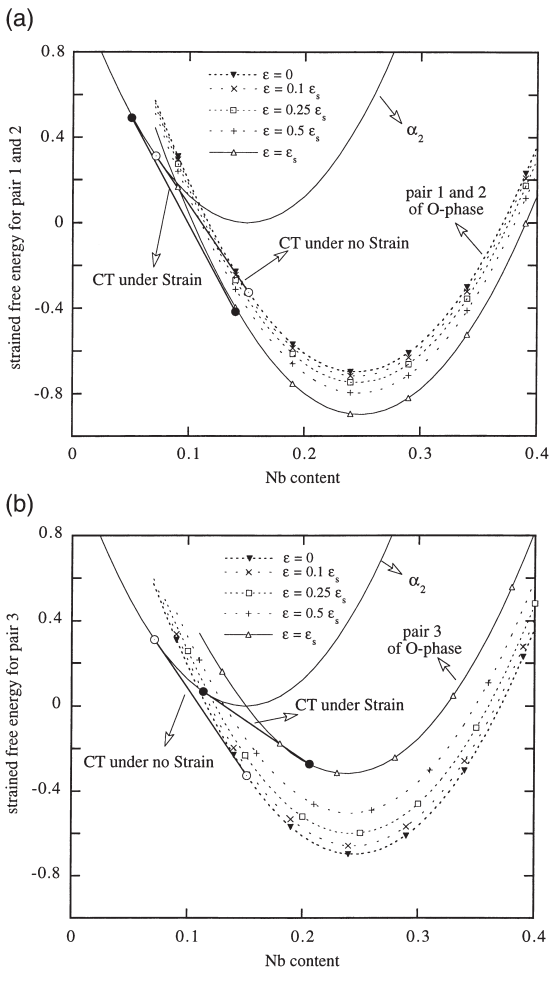

Fig. 8. Influence of applied strain on the free energy: (a) for pair 1 or 2; (b) for pair 3. The solid lines denote the common tangent, which is abbreviated as "CT" in the figure.

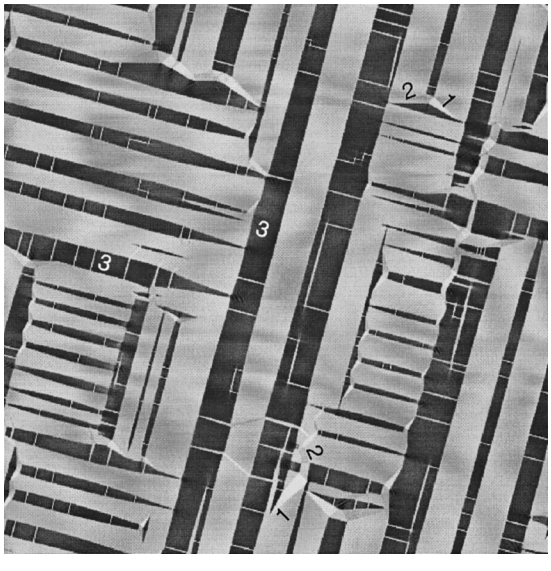

Fig. 9. Microstructure at $\tau = 200$ with a compressional applied strain of $0.5\epsilon_s$. Three pairs of the orientation variants are indicated in the figure.

suppress pairs 1 and 2, the microstructure consists of predominantly pair 3 and the parent phase, the amount of pairs 1 and 2 being negligible (less than 2%). The total volume fraction of the *O*-phase is ~34%, which is about one-half of that predicted under tensile strain. It is also lower than the equilibrium volume fraction predicted for the stress free system (e.g. 37% for alloy 2).

4. SUMMARY

The effect of an externally applied strain field on the equilibrium volume fraction of the product phase and microstructural patterns formed during a coherent α_2 to *O*-phase precipitation process in the Ti–Al–Nb system is investigated numerically using the phase field model. Two alloys with differing Nb content are considered and hence different volume fractions of the *O*-phase. When the applied strain is 1/10 of the shear magnitude of the stress free strain, the microstructural patterns are not greatly altered, although selective growth of orientation variants is obvious. With further increases in the applied field, selective growth becomes more intensive and the elastic strain energy becomes dominant over the chemical free energy, leading to very similar microstructures in the two alloys with differing Nb content. A single-phase structure of the *O*-phase can be obtained for both alloys when the applied strain field is of the same magnitude as the shear deformation of the *O*-phase.

Acknowledgements—This work is supported by NSF under grant DMR-96-33719 (Wen and Chen) and DMR-9703044 (Wen and Wang). The simulation was performed at the San Diego Supercomputer Center and the Pittsburgh Supercomputing Center (DMR940015).

REFERENCES

1. Muraleedharan, K. and Banerjee, D., *Phil. Mag. A*, 1995, **71**, 1011.
2. Muraleedharan, K. and Banerjee, D., *Scripta metall.*, 1993, **29**, 527.
3. Pierron, X., De Graef, M. and Thompson, A. W., *Phil. Mag. A*, 1998, **77**, 1399.
4. Wen, Y.H., Wang, Y., Bendersky, L.A. and Chen, L.Q. *Acta metall.*, 2000, **48**, 4125.
5. Wen, Y.H., Wang, Y. and Chen, L.Q., *Phil. Mag. A*, 2000, **80**, 1967.
6. Wen, Y. H., Wang, Y. and Chen, L. Q., *Acta metall.*, 1999, **47**, 4375.
7. Lifshitz, E. M. and Pitaevskii, L. P., *Statistical Physics*, Pergamon Press, Oxford, 1980.
8. Bendersky, L. A., Roytburd, A. and Boettinger, W. J., *J. Res. Natl. Inst. Stand. Technol.*, 1993, **98**, 561.
9. Khachaturyan, A. G., *Theory of Structural Transformations in Solids*. John Wiley & Sons, New York, 1983.
10. Li, D. Y. and Chen, L. Q., *Acta mater.*, 1998, **46**, 639.
11. Chen, D. Q. and Jie, S., *Comput. Phys. Commun.*, 1998, **108**, 147.
12. Bendersky, L. A., *Scripta metall.*, 1993, **29**, 1645.
13. Larché, F. C. and Cahn, J. W., *Acta metall.*, 1985, **33**, 331.
14. Johnson, W. C., Influence of Elastic Stress on Phase Transformations, in *Lectures on the Theory of Phase Transformations*. TMS-AIME, New York, 1999.